UC Berkeley
UC Berkeley Previously Published Works

Title
Controlled Isotropic and Anisotropic Shell Growth in β–NaLnF4 Nanocrystals Induced by Precursor Injection Rate

Permalink
https://escholarship.org/uc/item/6tp264m9

Journal
Journal of the American Chemical Society, 139(35)

ISSN
0002-7863

Authors
Fischer, Stefan
Swabeck, Joseph K
Alivisatos, A Paul

Publication Date
2017-09-06

DOI
10.1021/jacs.7b07496

Peer reviewed

eScholarship.org Powered by the California Digital Library
University of California

JACS
JOURNAL OF THE AMERICAN CHEMICAL SOCIETY

Article

pubs.acs.org/JACS

Controlled Isotropic and Anisotropic Shell Growth in β-$NaLnF_4$ Nanocrystals Induced by Precursor Injection Rate

Stefan Fischer,[†,‡] Joseph K. Swabeck,[†,‡] and A. Paul Alivisatos*[,†,‡,§,∥]

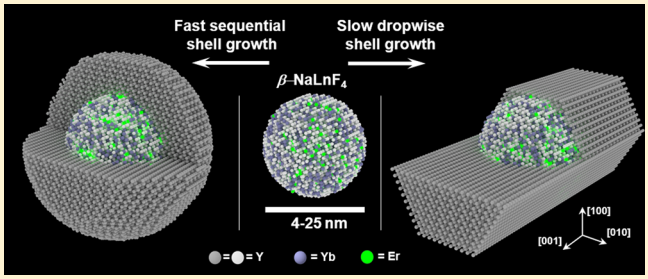
[†]Materials Sciences Division, Lawrence Berkeley National Laboratory, Berkeley, California 94720, United States

[‡]Department of Chemistry and [§]Department of Materials Science and Engineering, University of California—Berkeley, Berkeley, California 94720, United States

[∥]Kavli Energy NanoScience Institute, Berkeley, California 94720, United States

Supporting Information

ABSTRACT: Precise morphology and composition control is vital for designing multifunctional lanthanide-doped core/shell nanocrystals. Herein, we report controlled isotropic and anisotropic shell growth techniques in hexagonal sodium rare-earth tetrafluoride (β-$NaLnF_4$) nanocrystals by exploiting the kinetics of the shell growth. A drastic change of the shell morphology was observed by changing the injection rate of the shell precursors while keeping all other reaction conditions constant. We obtained isotropic shell growth for fast sequential injection and a preferred growth of the shell layers along the crystal's *c*-axis [001] for slow dropwise injection. Using this slow shell growth technique, we have grown rod-like shells around different almost spherical core nanocrystals. Bright and efficient upconversion was measured for both isotropic and rod-like shells around β-$NaYF_4$ nanocrystals doped with Yb^{3+}/Er^{3+} and Yb^{3+}/Tm^{3+}. Photoluminescence upconversion quantum yield and lifetime measurements reveal the high quality of the core/shell nanocrystal. Furthermore, multishell rod-like nanostructures have been prepared with optically active cores and tips separated by an inert intermediate shell layer. The controlled anisotropic shell growth allows the design of new core/multishell nanostructures and enables independent investigations of the chemistry and physics of different nanocrystal facets.



INTRODUCTION

Controlling the morphology of nanocrystals (NCs) is one of the main strategies to engineer the properties of NCs for specific requirements and applications. For example, changing the size and shape of NCs has been used to tune the band gap and polarizability of semiconductor NCs,[1] to alter the plasmonic behavior of metal nanoparticles,[2,3] or to modify the magnetic and optical properties of lanthanide-doped NCs.[4,5] Further freedom of design is given by additional shell layers of different materials or compositions to either improve desired features of the core NCs or create new interesting properties that are unique to core/shell nanostructures.[6−8]

Lanthanide-doped NCs offer manifold ways of optical engineering because of the wide range of atomic-like transitions in the divalent and trivalent lanthanide ions in combination with the easy exchange of different ions in a host crystal owing to their similar ionic radii.[9−11] Careful design of multiple shells in lanthanide-doped NCs led to the discovery of novel properties, such as temporally full color emission in a single NC by engineering energy transfer processes and controlling of doping profiles or surface quenching assisted downshifting processes by optimizing the passivation layers.[6,7,10,12]

Sodium rare-earth tetrafluoride ($NaLnF_4$) NCs are among the most studied host materials for lanthanide ions with respect to spectral conversion due to their favorable properties, such as low phonon energies, resulting in high spectral conversion efficiencies. In particular, the hexagonal (β-phase) crystal structure of $NaLnF_4$ is known for its excellent upconversion performance.[4,13,14] Shape control in core β-$NaLnF_4$ NCs is well understood.[15−18] Almost spherical NCs, nanoprisms, nanorods, or nanoplates can be grown by changing the reaction conditions, such as temperature, pH value, surfactant, or sodium, as well as fluorine, precursor concentration, ratio, and source.[15,17−20]

There is an enormous amount of research on lanthanide-doped core/shell NCs with inert shells[4,7,21−26] as well as active shells.[12,27−30] We refer to review articles for a more complete literature overview.[15,24,31−34] In general, one can categorize two different kinds of shelling methods for β-$NaLnF_4$ NCs. One set of methods is centered around seed-mediated heat-up procedures, where the previously synthesized core NCs are redispersed in a new solution containing the shell precursors.[35,36] By heating up the solution, the shell precursors grow onto the previously synthesized NCs and form a shell layer. This procedure can be repeated multiple times. The other set of methods is based on the injection of shell precursors into the reaction flask at elevated temperatures. For the β-$NaLnF_4$ NCs,

Received: July 18, 2017
Published: August 4, 2017

© 2017 American Chemical Society

DOI: 10.1021/jacs.7b07496
J. Am. Chem. Soc. 2017, 139, 12325−12332

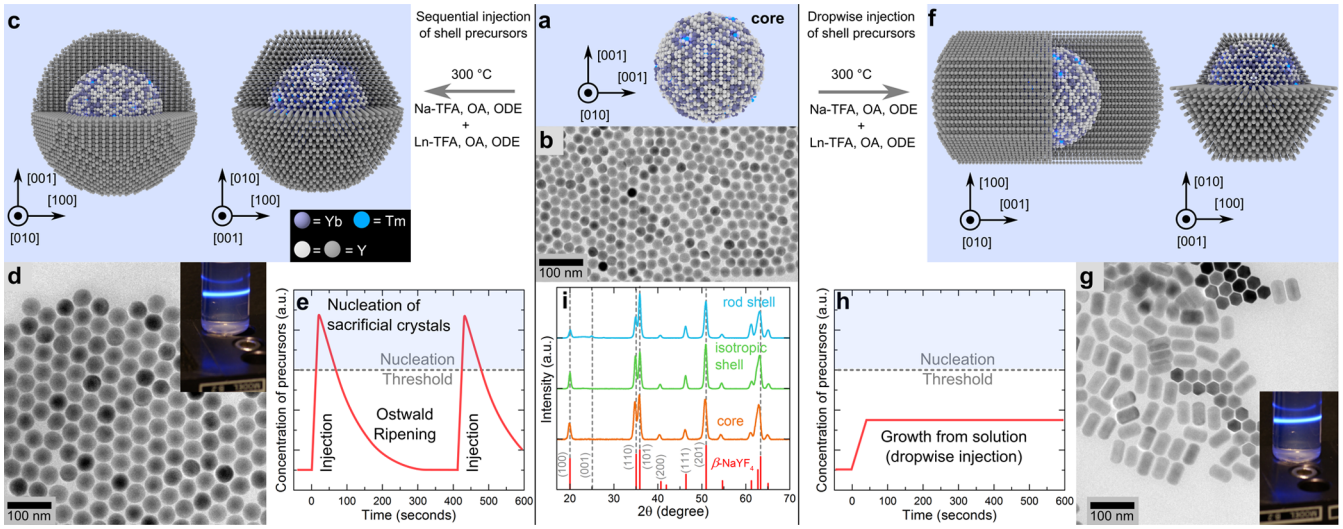


Figure 1. (a,b) Schematic and TEM images of β-$NaYF_4$:Yb^{3+},Tm^{3+} core NCs. (c) Schematic and (d) TEM image of core/shell NCs in which the β-$NaYF_4$ shell was grown by sequential injection of the shell precursor. (e) Rapid increase of the shell precursor concentration above the nucleation threshold results in the growth of small NCs, which then ripen onto the larger core NCs in the solution. (f) Schematic and (g) TEM image of the core/shell NC in which the β-$NaYF_4$ shell was grown by continuous dropwise injection of the shell precursor. (h) In this slow injection regime, the concentration of shell precursors is below the nucleation threshold, and the different growth rates at the different facets result in anisotropic shell growth. The insets in (d) and (g) show photographs of the blue upconversion luminescence under 980 nm laser excitation (41 W/cm^2). (i) X-ray diffraction patterns confirm the pure hexagonal phase of the NCs shown in (b), (d), and (g).

one can distinguish between two kinds of hot injection methods, one in which previously synthesized small sacrificial NCs are injected and subsequently ripen onto the core NCs[37,38] and another one where the shell precursors are injected directly into the hot reaction vessel.[39,40] Both of these techniques have demonstrated epitaxial and mostly isotropic shell growth for tensile strained core to shell interfaces resulting, for example, in high quality upconverting NCs.[23,37,40−42] However, often elliptical shells around almost spherical cores are reported, although an isotropic shell was desired.[6,10] The focus in these studies was mostly set on optical properties, and little attention was given to the morphology of the core/shell NCs.[6,10] Despite the huge efforts undertaken, controlling the shape of the shell is still not yet fully understood.[24]

There is a number of articles reporting shape-controlled shell growth around β-$NaLnF_4$ microcrystals and NCs.[8,20,43−46] In all of these studies and very similar to the case of core NCs, shape control of the shell is achieved by changing the reaction conditions such as temperature, pH, concentration, and source of sodium and fluorine, surfactant (typically oleic acid vs oleate ratio), and using different rare-earth ions for the shell growth. The growth rate of the shell layer as well as the injection rate of the shelling precursors is widely overlooked as a parameter affecting the shell growth.

Here, we investigate changes of the shell morphology under identical reaction conditions with variations only in the injection rate of the shell precursor. Using either a fast sequential or slow dropwise shell growth technique, we observed significant morphology changes of the shell layers and obtained isotropic or rod-like shells around almost spherical core β-$NaLnF_4$ NCs, respectively. The core/shell NCs are monodisperse and show high optical quality. This controlled directional shell growth enables designing of anisotropic multishell nanostructures, such as a dot−rod−tip architecture, which may enable novel properties due to selected passivation of certain crystal facets or confined energy migration pathways, for example, along the crystal's *c*-axis [001].

RESULTS AND DISCUSSION

In this study, we follow the previously mentioned second type of hot injection methods for β-$NaLnF_4$ NCs by injecting shell precursor solutions of lanthanide trifluoroacetate (Ln-TFA) and sodium trifluoroacetate (Na-TFA) dissolved in oleic acid (OA) and 1-octadecene (ODE). In related literature methods, sodium oleate and Ln-TFA are injected in an alternating manner to grow shell layers.[40] In our approach, we mixed the individually prepared Na-TFA and Ln-TFA precursor solutions to inject both at the same time. We investigate the shell growth under different injection conditions of the shell precursor for the same reaction conditions. Fast sequential injection of the shell precursor resulted in more isotropic shell growth, whereas rod-like shells were grown using slow dropwise injection of the shell precursor as shown in Figure 1 and discussed below.

Core β-$NaYF_4$ NCs doped with Yb^{3+} and Er^{3+} or Tm^{3+} were synthesized for upconversion (UC) of 980 nm near-infrared (NIR) photons to visible and/or NIR photons following literature methods using Ln-acetates.[7,19,37] In the first approach, we shelled almost spherical β-$NaYF_4$:Yb^{3+},Tm^{3+} NCs with a diameter of 23.7 ± 1.2 nm as shown in the schematic of Figure 1a and the transmission electron microscopy (TEM) image in Figure 1b. We always used the unwashed reaction solution of the core NCs for the shelling procedures. In a reaction, a volume of 11 mL (0.5 mmol) of the β-$NaYF_4$:25% Yb^{3+},0.5% Tm^{3+} core NC stock solution was transferred into a 50 mL four-neck flask. The solution was heated to 300 °C in 7 min under argon flow and vigorous stirring. The shelling procedure was started once the solution reached 300 °C.

For isotropic shell growth, an amount of 0.3 mmol of the shell precursor solution was added in a rapid injection. This sequence was repeated five times with a waiting period between injections of 8 min. The schematic in Figure 1c illustrates the core/shell structure. Figure 1d shows a TEM image of the

DOI: 10.1021/jacs.7b07496
J. Am. Chem. Soc. 2017, 139, 12325−12332

core/shell NCs with isotropic shells and a size distribution of 39.9 ± 2.4 nm. In this sequential method, the amount of shell precursors in the reaction flasks exceeds the nucleation threshold, resulting in a nucleation burst of small sacrificial NCs which will ripen quickly onto the core NCs (Figures S4 and S5). Immediately after injection, monomers will also grow directly onto the core NCs, resulting in an increased size distribution which will focus and narrow down to $\sigma \leq 7\%$ by Ostwald ripening of the sacrificial NCs. Isotropic shells and monodisperse core/shell β-$NaLnF_4$ NCs are obtained using this sequential method.[7]

The shell growth is altered drastically by injecting the shell precursors continuously and dropwise, as shown in the schematic of Figure 1f and the TEM image in Figure 1g. We used the same composition and amount of shell precursor (1.5 mmol) as before in the sequential method but injected it over 1.5 h with a constant rate of 1 mmol/h (2 mmol/h for 1 mmol of core NCs) using a mechanical syringe pump. This means that after 1 h a shell with approximately twice the volume of the core NCs will be grown. Because of the slow injection, the monomer concentration never exceeds the nucleation threshold (Figure 1h). Consequently, the decomposed shell precursors grow directly on the NCs. Oleate ligands (OA^-) bind more strongly than oleic acid ligands (OAH) on β-$NaYF_4$.[45] Furthermore, the binding energy of oleate ligands at the (100) and (010) facets of −35.4 meV/Å^2 is 63% higher than the (001) binding energies.[45] Consequently, it is energetically favorable to grow on the (001) facet and therefore along the crystal's *c*-axis, resulting in rod-like shells. All samples show pure hexagonal crystal structure (Figure 1i). The observation of more isotropic shell growth due to fast sequential injection may be a consequence of the larger number of precursors that may result in similar growth rates on all facets. Nucleation followed by Ostwald ripening may also contribute to the more isotropic shell growth.[37]

Both shell geometries result in bright upconverting particles, as shown in Figure 1 with blue emission from the Tm^{3+} transitions $^1G_4 \rightarrow {}^3H_6$ and $^1D_2 \rightarrow {}^3F_4$ (Figure 2a). Both samples show the same emission spectra under 41 W/cm^2 excitation using a 980 nm laser with the brightest emission at 800 nm from $^3H_4 \rightarrow {}^3H_6$ (Figure 2b). In addition, we measured lifetimes of the Yb^{3+} $^2F_{5/2} \rightarrow {}^2F_{7/2}$ transition, 899 μs for isotropic and 873 μs for rod-like shell, as well as the UC emission of the Tm^{3+} $^3H_4 \rightarrow {}^3H_6$ transition, 819 μs for isotropic and 815 μs for rod-like shell (Figure 3a). These very similar lifetimes reveal similar passivation of the active core by both isotropic and rod-like shells. This observation is somewhat surprising because it is commonly accepted that isotropic shells should result in better passivation, which leads to less surface quenching (nonradiative relaxation) and therefore longer lifetimes. However, upconversion quantum yield (UCQY) measurements show the expected trend of higher values for the isotropic shell (Figure 3b). We determined UCQY values up to 5.8 ± 0.5% for the isotropic shell and 4.7 ± 0.6% for the rod-like shell for the upconversion from 980 to 800 nm at 41 ± 3 W/cm^2. The UCQY value for the blue emission of both the samples is roughly 1.6% of the 980 to 800 nm value. As in a previous study,[7] emission from the Yb^{3+} $^2F_{5/2} \rightarrow {}^2F_{7/2}$ transition overlapping with the 980 nm excitation was considered in the UCQY analysis. This background correction results in higher absorptance by the sample and therefore lower UCQY values. Here, the UCQY value of the isotropic sample was reduced by 34% from an absolute value of 8.8% by considering the Yb^{3+} $^2F_{5/2} \rightarrow {}^2F_{7/2}$ emission background.

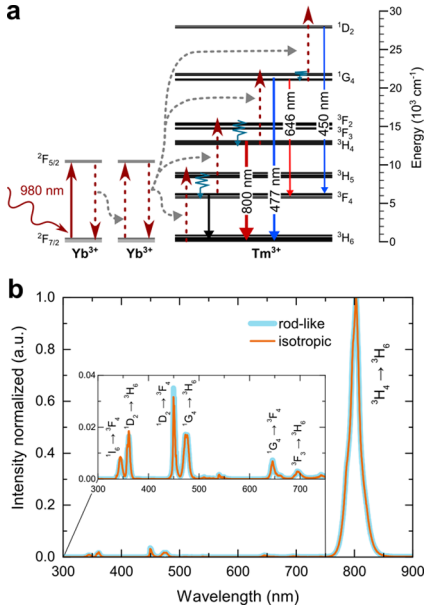


Figure 2. (a) Simplified energy level diagram and proposed mechanism for UC of 980 nm photons in β-$NaYF_4$:Yb^{3+},Tm^{3+}. The strongest UC luminescence from the $^3H_4$ energy level around 800 nm originates from a two-photon process, whereas the weaker blue emissions are based on three- and four-photon pathways. (b) β-$NaYF_4$:25% Yb^{3+},0.5% Tm^{3+} NCs with isotropic and rod-like shells have almost identical UC emission spectra under 980 nm excitation.

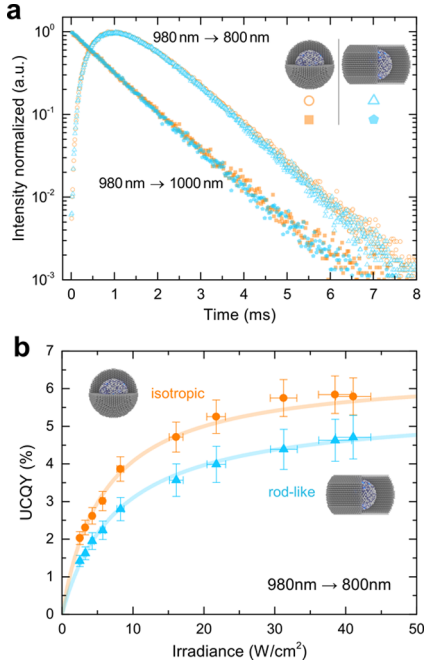


Figure 3. (a) Very similar lifetimes were measured for β-$NaYF_4$:25% Yb^{3+},0.5% Tm^{3+} NCs with isotropic and rod-like shells in cyclohexane. The determined decay times for the Yb^{3+} $^2F_{5/2} \rightarrow {}^2F_{7/2}$ transition (980 nm → 1000 nm) are 899 and 873 μs, and the UC emission from Tm^{3+} $^3H_4 \rightarrow {}^3H_6$ transition (980 nm → 800 nm) is 819 and 815 μs for isotropic and rod-like shells, respectively. (b) UCQY from 980 to 800 nm shows a steep rise at low irradiance values with higher values for the isotropic shell.

DOI: 10.1021/jacs.7b07496
J. Am. Chem. Soc. 2017, 139, 12325−12332

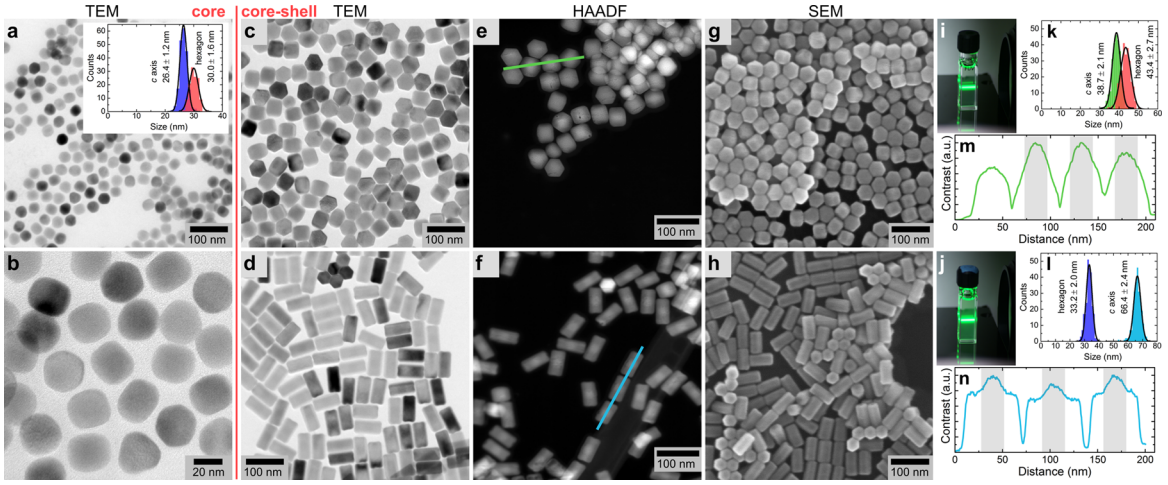


Figure 4. Electron microscope images of β-$NaYF_4$:Yb^{3+},Er^{3+} NCs with fast sequential and slow dropwise grown β-$NaYF_4$ shells. (a,b) TEM images and size distribution of the β-$NaYF_4$:Yb^{3+},Er^{3+} core NCs. (c,d) TEM, (e,f) HAADF, and (g,h) SEM images of β-$NaYF_4$:Yb^{3+},Er^{3+} NCs with β-$NaYF_4$ shells grown using sequential or slow dropwise injection, respectively. The photographs in (i) and (j) show the UC luminescence of the isotropic and rod-like UCNCs in cyclohexane under 980 nm (30 W/cm^2) excitation. (k,l) Narrow size distributions ($\sigma \leq 7\%$) are determined for the short axis/hexagon as well as the long axis/*c*-axis [001]. (m,n) Contrast line scans of the HAADF image as indicated in (e,f). The cores are located in the center of the nanocrystals, as indicated by the gray areas.

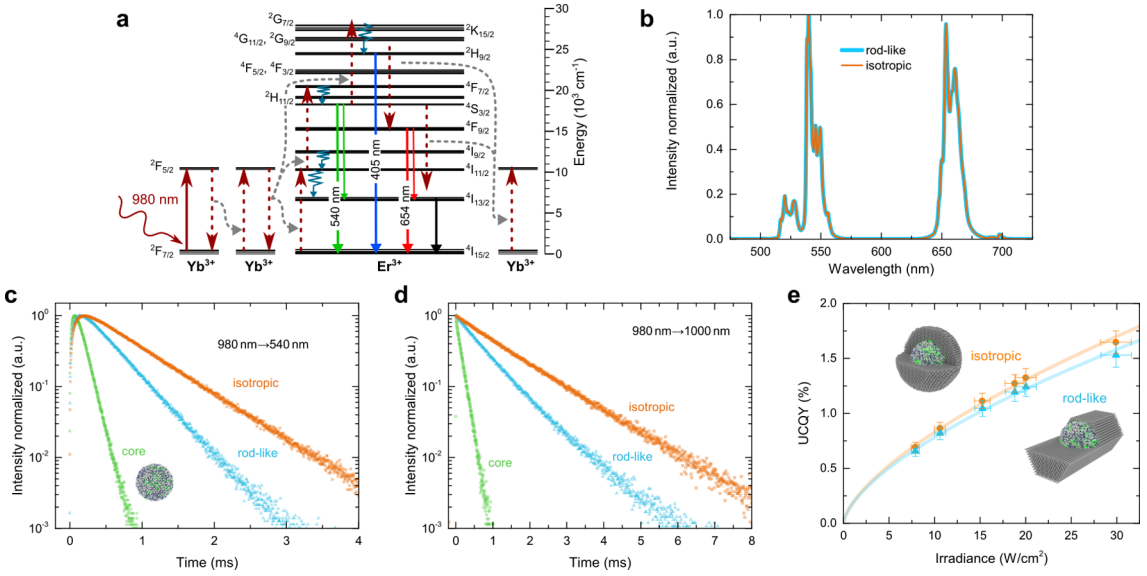


Figure 5. (a) Simplified energy level diagram and proposed mechanism for UC of 980 nm photons in β-$NaYF_4$:Yb^{3+},Er^{3+}. (b) UC emission spectra for isotropic and rod-like shell morphology are almost identical with dominant emission from the energy levels $^4S_{3/2}$ (green) and $^4F_{9/2}$ (red) to the ground state $^4I_{15/2}$. (c,d) Photoluminescence lifetime measurements reveal the improved passivation of an isotropic shell over a rod-like inert shell in comparison to the bare core sample. (e) Very similar UCQY values were measured for both morphologies.

Next, we used slightly faceted β-$NaYF_4$:30% Yb^{3+},4% Er^{3+} core NCs (Figure 4a,b) and grew β-$NaYF_4$ shells around these crystals. We choose this lanthanide doping because of the high UCQY values, which we measured in a previous study.[7] Both core/shell NCs are purely hexagonal phase (Figure S6). The structure and composition of the NCs were investigated with different electron microscopy techniques. TEM images show the 2D representation of the NCs (Figure 4c,d). The size distribution was determined from TEM images of the isotropic but still faceted core/shell NCs (Figure 4k) and the rod-like NCs (Figure 4l). The rod-like core/shell nanocrystals have an aspect ratio of 1:2. High-angle annular dark-field (HAADF)-STEM features higher contrast between the yttrium ions and much heavier lanthanide ions. This technique was used to locate the core in the core/shell NCs (Figure 4e,f). Contrast line scans on the HAADF images show the centered position of the core inside the core/shell structure (Figure 4m,n). In addition, SEM was used to image the surface of the NCs, which shows a more three-dimensional representation of the NCs (Figure 4g,h). The drastic morphology changes can also be observed in other rare-earth host crystals and smaller NCs, as shown in the Supporting Information for roughly 4 nm β-$NaGdF_4$:20% Yb^{3+},2% Er^{3+} NCs (Figure S11).

The β-$NaYF_4$:30% Yb^{3+},4% Er^{3+} core/shell samples show bright green and red UC emission under 980 nm laser excitation (Figure 4i,j). The efficient passivation of the core by the β-$NaYF_4$ shell layers was confirmed by photoluminescence lifetime and UCQY measurements (Figure 5). We measured

DOI: 10.1021/jacs.7b07496
J. Am. Chem. Soc. 2017, 139, 12325−12332

lifetimes of the Yb^{3+} $^2F_{5/2} \rightarrow {}^2F_{7/2}$ transition of 727 and 1278 μs as well as UCQY values of 1.5 ± 0.1 and 1.6 ± 0.1% under 30 ± 2 W/cm^2 for the rod-like and the isotropic core/shell NCs, as shown in Figure 5, respectively. The lifetime of the Yb^{3+} $^2F_{5/2} \rightarrow {}^2F_{7/2}$ transition in the rod-like shell NCs already reaches a value where we had observed a saturation of the UCQY versus shell thickness in our previous study reported in ref 7. The small improvement of the UCQY despite the significant improvement of the lifetime shown here is in agreement with these previous results.

Rod-like core/shell NCs feature interesting additional options for multishell structures. For example, the distance between rare-earth ions along [001] is the shortest in the hexagonal crystal structure. Therefore, energy migration is most efficient in this direction because of the higher probability of dipole−dipole energy transfer between neighboring lanthanide ions which scales with d^{-6}. Furthermore, compared to an isotropic shell, the energy migration volume in the shell is reduced, resulting in less shell material necessary for an active energy migration layer which is often used in dye-sensitized upconverter systems to improve their efficiency.[12] Dropwise and sequential shell growth can also be combined to create even more complex anisotropic core/shell structures.

As a proof of concept, we synthesized core/multishell NCs with combined dropwise and sequential injections starting with 1 mmol of the β-$NaYF_4$:Yb^{3+},Er^{3+} core NCs from Figure 4a,b. First, we grew a rod-like β-$NaYF_4$ shell (Figure 6a, CS1) by injecting 1.5 mmol of the corresponding shell precursors in 1 h. After this first injection, we allowed the reaction to cool to room temperature (RT) and subsequently added a quarter of the solution into a new 25 mL four-neck reaction flask. Next, the solution was heated again to 300 °C under argon flow, and a β-$NaYF_4$:10% Tm^{3+} tip was grown onto the rod-like core−shell NCs (Figure 6b, CS2) by injecting 0.5 mmol of the corresponding shell precursors dropwise over 1 h. After a sample of half the solution was extracted out of the hot reaction vessel, we used Na-TFA and Lu-TFA precursors to grow a passivation shell around the dot−rod−tip NCs using the sequential injection method (Figure 6c, CS3). In total, 0.55 mmol of Na-TFA and Lu-TFA shell precursors were used in three subsequent injections with 8 min intervals. The size distributions of the short and long axes of the rod-like core/shell NCs show the dominant shell growth along [001] during dropwise injection and more isotropic growth of the β-$NaLuF_4$ shell layer by sequential injections (Figure 6d). After growing the β-$NaYF_4$:10% Tm^{3+} tip, the short axis lengthened by only 1 nm, whereas the growth at the long axis was 15.9 nm.

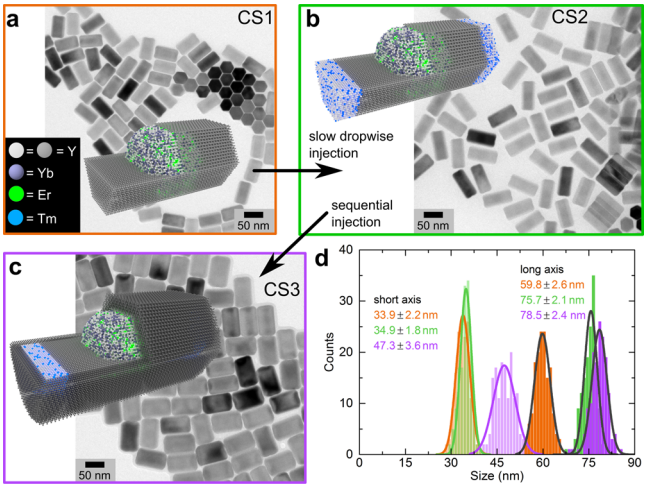


Figure 6. (a) Rod-like β-$NaYF_4$ shell was grown around the β-$NaYF_4$:Yb^{3+},Er^{3+} core NCs shown in Figure 4a,b. (b) At the tips of the rod-like NCs, β-$NaYF_4$:10% Tm^{3+} was grown by further dropwise injection of the corresponding shell precursors. (c) Using fast sequential injections, a shell of β-$NaLuF_4$ was grown around the complete dot−rod−tip NCs. (d) Size distributions of the short and long axes of the core/shell NCs showing preferred growth along [001] for dropwise and isotropic growth for sequential injection.

We chose the highly Tm^{3+}-doped tip to study potential diffusion of lanthanide ions through the NCs. If Yb^{3+}, Er^{3+}, or Tm^{3+} ions diffuse through the NC, we should see some UC emission at 800 nm. The absence of any 800 nm emission from Tm^{3+} in the UC spectra at 980 nm excitation suggests no significant diffusion of Ln^{3+} in our shelling procedure (Figure S13). We note that this, while not definitive, does imply that there is no significant diffusion of the lanthanide ions in the nanocrystals. In addition, we used excitation spectra as another indirect verification of the separation between the core and the tip of the NCs (Figure S13). Whereas luminescence at 980 nm originates from the $^4I_{11/2}$ Er^{3+} and the $^2F_{5/2}$ Yb^{3+} energy levels, luminescence at 800 nm is efficiently emitted from the $^3H_4$ Tm^{3+} energy level (Figure 3e). No difference in the excitation spectra between the three structures (CS1, CS2, and CS3) was determined for 980 nm emission originating from the $^4I_{11/2}$ Er^{3+} and the $^2F_{5/2}$ Yb^{3+} energy levels of the core. On the other hand, significant differences were observed for the 800 nm emission mostly emitted from the $^3H_4$ Tm^{3+} energy level of the tip (Figure S13). These observations suggest no coupling between Tm^{3+} and Er^{3+} ions in the tip and the core. Another dot−rod−tip structure with combined upconverter in the core and Ce^{3+},Tb^{3+} UV-to-green downshifter in the tip supports our findings of successful lanthanide separation despite the long shelling reaction times of >2.5 h at 300 °C (Figure S14).

We provided a shelling technique that allows the morphology of the epitaxial shell layer to change solely on the injection kinetics of liquid shell precursor without any other modifications on the reaction conditions. Using the shelling technique presented, high-quality core/shell UCNCs were synthesized with UCQY values comparable to previous studies with isotropic β-$NaLuF_4$ shells.[7] A layer-by-layer shell growth was demonstrated for the rod-like shell growth with different lanthanide ions at the tip of the core/multishell structures. This opens a novel way of engineering β-$NaLnF_4$ core/multishell nanostructures and may allow investigations of the different facets more independently.

■ CONCLUSIONS

We studied the role of the injection kinetics of identical liquid shell precursors, which are lanthanide trifluoroacetates and sodium trifluoroacetate dissolved in oleic acid and 1-octadecene, on the epitaxial shell growth on β-$NaLnF_4$ nanocrystals while keeping all other reaction conditions the same. We observed a drastic change in the shell morphology by exploiting slow dropwise and fast sequential shell growth techniques. On the one hand, fast sequential injection of the shell precursor results in isotropic shell growth. The rapid increase of the shell precursor in the reaction vessel and their quick decomposition results in a nucleation burst of small nanocrystals. These nanocrystals will ripen onto the bigger NCs that were previously in the solution, resulting in more isotropic

DOI: 10.1021/jacs.7b07496
J. Am. Chem. Soc. 2017, 139, 12325−12332

growth. On the other hand, slow dropwise injection of the shell precursors results in rod-like shell morphologies. Here, the concentration of shell precursors does not exceed the nucleation threshold. The shell grows preferably onto the (001) facet because of the stronger binding energies of the oleate ligands at the (010) and (100) facets. Both shelling methods result in nanocrystals with high crystal quality and narrow size distributions. The flexibility of the procedure allows layer-by-layer shell growth and also the design of complex anisotropic multishell structures, such as the introduced dot−rod−tip structure with an optically active core and tip.

MATERIALS AND METHODS

Chemicals. Yttrium acetate hydrate (99.9%), ytterbium acetate hydrate (99.95%), erbium acetate hydrate (99.9%), thulium acetate hydrate (99.9%), gadolinium acetate hydrate (99.9%), sodium trifluoroacetate (98%), sodium hydroxide (≥98%), ammonium fluoride (≥99.9%), 1-octadecene (90%), and oleic acid (90%) were purchased from Sigma-Aldrich. All rare-earth oxides (99.9%) and trifluoroacetic acid (99%) were purchased from Alfa Aesar. Sodium oleate was purchased from TCI America. All the chemicals were used as received without further purification.

Synthesis of the Doped and Undoped β-$NaYF_4$ Core Samples. β-$NaLnF_4$ core nanocrystals have been synthesized as reported by Li et al. with small modifications.[19] For the desired doping level, the corresponding molar ratios of the rare-earth acetate precursors were charged into a three-neck flask. For molar amounts of 1−1.5 mmol, a 100 mL flask was used, whereas a 250 mL flask was used for larger amounts, up to 5 mmol. The acetates were mixed with 5.5 mL of oleic acid and 17 mL of 1-octadecene for each mmol of rare-earth acetate precursors. The solution was heated to 120 °C under vacuum until it turned translucent after approximately 1 h. Then, the solution was cooled to RT. Subsequently, for each mmol of acetate precursor in the flask, a clear mixture of 8 mL of methanol, 4 mmol of NH_4F, and 2.5 mmol of NaOH was added dropwise into the reaction vessel and stirred for 60 min at RT. Afterward, the mixture was heated to 70 °C while open to the atmosphere to remove the methanol. Then the solution was heated to 100 °C under argon flow to remove residual water before the solution was heated in 10 min to 300 °C (rate of ∼20 °C/min) under argon flow. The mixture was kept at that temperature for 60 min for amounts up to 1.5 mmol and 90 min for larger amounts with constant, moderate stirring. Next, the heating mantle was removed to let the solution cool to RT. The unwashed solution was used for the later shelling. We stored such core solutions stirring at RT for more than 2 months without any sign of degradation.

A small amount was removed out of the flask and kept as the core sample for the later experiments. This sample was precipitated and subsequently washed by dispersing the NCs in small amounts of hexane, precipitated by addition of ethanol, and collected by centrifugation (1800*g*) two times before they were dispersed in cylcohexane.

Shelling Precursor Solutions. The shelling precursor solutions were prepared by the following standard procedure. First, we dissolved a ratio of 1 mmol rare-earth oxides, for example, Y_2O_3, in 1 mL of 99% trifluoroacetic acid and 5 mL of distilled water in a 50 or 100 mL three-neck flask. This mixture was heated to 90 °C for more than 6 h in an oil bath using a condenser column to prevent evaporation. After all the Y_2O_3 was dissolved and the solution was transparent, the water and the remaining trifluoroacetic acid were evaporated at 65 °C to obtain a white powder of 2 mmol yttrium trifluoroacetate. Next, we added 3 mL of oleic acid and 3 mL of 1-octadecence into the flask. The mixture was heated carefully under vacuum to 120 °C to obtain a clear, slightly yellow solution. After cooling the mixture to 50 °C, we transferred the slightly viscous precursor liquid into a vial for later use (Figure S1). The same procedure can also be used with other rare-earth oxides to prepare rare-earth shelling precursors of all trivalent rare-earth ions. Lutetium precursor solutions turned out to be very viscous, so an additional 0.5 mL of OA and ODE was added for each mmol of shell precursor.

In another three-neck flask, we mixed 2 mmol of sodium trifluoroacetate ($NaCF_3CO_2$), 1.5 mL of oleic acid, and 1.5 mL of 1-octadecence and heated the solution carefully to 120 °C under vacuum. After the $NaCF_3CO_2$ was completely dissolved and the solution became clear, the heating was turned off. The liquid was transferred into a vial at RT. We found no sign of degradation of the rare-earth and sodium shell precursors after storing them at RT in the dark for more than 6 months.

The rare-earth and sodium precursor solutions were mixed into a vial on a hot plate (between 50 and 100 °C) while stirring with a 1:1 molar ratio to obtain the final shelling precursor solution for injection. This shelling precursor solution was prepared shortly before the injection to grow the shell as described below.

Shell Growth by Slow Dropwise Injection. We added a certain amount of the unwashed core stock solution into a four-neck flask. Depending on the amount, 25, 50, 100, or 250 mL flasks were used. Here, we describe the method for an amount of 0.5 mmol (∼11 mL) of the core stock solution in a 50 mL flask. 1-Octadecene can be added to the stock solution to dilute the nanocrystal concentration. The mixture was degassed under vacuum before heating to 300 °C. After quickly heating the solution within around 7 min to 300 °C under argon flow, we started the shelling procedure immediately, in which we injected the liquid shell precursors dropwise into the reaction vessel using a mechanical syringe pump. We used the fourth neck of the flask for the injection. Typically, the desired amount of shell precursor was injected with rates between 1 and 3 mmol/h for every mmol of core (or core/shell nanocrystal) in the solution at the beginning of the shelling procedure to obtain rod-like shell growth. Essentially, this rate measure means that the volume of the NCs increases by factors of roughly 1−3 per hour due to the shell growth. Slower injection rates were chosen to make sure that the concentration of shelling precursor is below the nucleation limit. Faster injection rates were used, for example, when the core solution sample from the stock solution (as described above) was diluted by addition of 1-octadecence. The solution was kept under slow, constant argon flow and moderate stirring. After the injection was finished, the solution was kept at the reaction temperature for another 10 min before the heating mantle was removed to let the solution cool to RT.

The nanocrystals in solution can either be used for further shelling−tip or other shell growth or washed and dispersed in an organic solvent. In this case, the nanocrystals were precipitated by addition of ethanol, collected by centrifugation (1800*g*), washed twice with small amounts of hexane and ethanol (centrifugation with 1800*g*), and finally dispersed in 8−10 mL of cyclohexane.

Shell Growth by Sequential Injections. Same starting procedure as described before was used in the dropwise shell growth. We started the shelling procedure immediately after the reaction temperature of 300 °C was reached. In a typical shelling sequence (0.5 mmol core solution), we injected 0.3 mmol of the shell precursor solution in one fast shot through the septum of the fourth neck of the flask. After a time of 5−10 min to let the TFA decompose to grow a β-$NaLnF_4$ shell, the described sequence was repeated. The solution was kept under slow constant argon flow and moderate stirring. After the final injection was finished, the solution was kept at the reaction temperature for another 10 min before the heating mantle was removed to let the solution cool to RT. The nanocrystals in solution can either be used for further synthesis experiments and additional shelling or washed as described before.

Material Characterization. TEM images were taken on a FEI Tecnai T20 equipped with a Gatan SC200 CCD camera and a LaB6 filament operated at 200 kV. STEM images were taken on a JEOL 2100-F 200 TEM at the Molecular Foundry. SEM images were taken on a Zeiss Gemini Ultra-55 with an acceleration voltage of 5 kV at the Molecular Foundry. X-ray diffraction patterns were obtained using a Bruker D-8 GADDS diffractometer equipped with a Co Kα.

Optical Characterization. Emission spectra and upconversion quantum yield measurements under 980 nm continuous wave excitation were performed with a custom-built integrating sphere

DOI: 10.1021/jacs.7b07496
J. Am. Chem. Soc. 2017, 139, 12325−12332

photoluminescence setup. This setup consists of a four-port integrating sphere (Labsphere Inc.), a Princeton Instruments SP2300 spectrometer equipped with a Si-CCD camera (Princeton Instrument, PIXIS 400B), which is thermoelectrically cooled to −55 °C, and an indium gallium arsenide (InGaAs) camera (Andor, iDus InGaAs 1.7 μm), which is thermoelectrically cooled to −85 °C. A 2 W continuous wave 980 nm laser (CNI, MDL-III-980) was used with power stability <0.185% over 4 h. Light exiting the integrating sphere passes through an 850 nm short-pass filter (Edmund Optics) to attenuate the 980 nm laser which would otherwise saturate our detector for an integration time of 1 s that was used for most measurements. The complete system was calibrated with a NIST-traceable radiometric calibration source (OceanOptics, HL-CAL-3plus, serial number 089440003, calibration number 19936).

For time-dependent measurements, we used a Nd:YAG pumped optical parametric oscillator, Opolette HE 355 LD from Opotek, in combination with a FLS980 fluorescence spectrometer from Edinburgh Instruments. Two photomultiplier tubes from Hamamatsu are attached: a TE-cooled R2658P with a spectral range from 200 to 1010 nm and a detector response of 800 ps, and a liquid-nitrogen-cooled R5509-72 with a spectral range from 300 to 1700 nm and a detector response of 800 ps. The complete system was calibrated for the sensitivity of all parts and all excitation detector combinations by Edinburgh Instruments.

More details can be found in the Supporting Information and ref 7.

■ ASSOCIATED CONTENT

Supporting Information

The Supporting Information is available free of charge on the ACS Publications website at DOI: 10.1021/jacs.7b07496.

Experimental details on the synthesis, material and optical characterizations, supplementary results and discussion (PDF)

■ AUTHOR INFORMATION

Corresponding Author

*paul.alivisatos@berkeley.edu

ORCID

Stefan Fischer: 0000-0003-4110-6576

Joseph K. Swabeck: 0000-0003-2235-2472

A. Paul Alivisatos: 0000-0001-6895-9048

Notes

The authors declare no competing financial interest.

■ ACKNOWLEDGMENTS

The authors thank Brent Koscher for synthesis advice and X-ray diffraction measurements. The work was supported by the Light−Material Interactions in Energy Conversion, an Energy Frontier Research Center funded by the U.S. Department of Energy, Office of Science, Office of Basic Energy Sciences, under Contract DE-AC02-05CH11231, part of the EFRC at Caltech under DE-SC0001293. Work at the Molecular Foundry was supported by the Office of Science, Office of Basic Energy Sciences, of the U.S. Department of Energy under Contract No. DE-AC02-05CH11231. S.F. gratefully acknowledges the scholarship support from the German Research Foundation (DFG, agreement FI 2042/1-1).

■ REFERENCES

(1) Hu, J.; Li, L.-s.; Yang, W.; Manna, L.; Wang, L.-w.; Alivisatos, A. P. *Science* **2001**, *292* (5524), 2060.

(2) Jain, P. K.; Lee, K. S.; El-Sayed, I. H.; El-Sayed, M. A. *J. Phys. Chem. B* **2006**, *110* (14), 7238.

(3) Rogobete, L.; Kaminski, F.; Agio, M.; Sandoghdar, V. *Opt. Lett.* **2007**, *32* (12), 1623.

(4) Boyer, J.-C. C.; van Veggel, F. C. J. M. *Nanoscale* **2010**, *2* (8), 1417.

(5) Johnson, N. J. J.; Oakden, W.; Stanisz, G. J.; Scott Prosser, R.; van Veggel, F. C. J. M. *Chem. Mater.* **2011**, *23* (16), 3714.

(6) Deng, R.; Qin, F.; Chen, R.; Huang, W.; Hong, M.; Liu, X. *Nat. Nanotechnol.* **2015**, *10* (3), 237.

(7) Fischer, S.; Bronstein, N. D.; Swabeck, J. K.; Chan, E. M.; Alivisatos, A. P. *Nano Lett.* **2016**, *16* (11), 7241.

(8) Zhang, Y.; Zhang, L.; Deng, R.; Tian, J.; Zong, Y.; Jin, D.; Liu, X. *J. Am. Chem. Soc.* **2014**, *136* (13), 4893.

(9) Dieke, G. H.; Crosswhite, H. M. *Appl. Opt.* **1963**, *2* (7), 675.

(10) Peng, D.; Ju, Q.; Chen, X.; Ma, R.; Chen, B.; Bai, G.; Hao, J.; Qiao, X.; Fan, X.; Wang, F. *Chem. Mater.* **2015**, *27* (8), 3115.

(11) Han, S.; Qin, X.; An, Z.; Zhu, Y.; Liang, L.; Han, Y.; Huang, W.; Liu, X. *Nat. Commun.* **2016**, *7*, 13059.

(12) Chen, G.; Damasco, J.; Qiu, H.; Shao, W.; Ohulchanskyy, T. Y.; Valiev, R. R.; Wu, X.; Han, G.; Wang, Y.; Yang, C.; Ågren, H.; Prasad, P. N. *Nano Lett.* **2015**, *15* (11), 7400.

(13) Suyver, J. F.; Grimm, J.; Krämer, K. W.; Güdel, H. U. *J. Lumin.* **2005**, *114* (1), 53.

(14) Goldschmidt, J. C.; Fischer, S. *Adv. Opt. Mater.* **2015**, *3* (4), 510.

(15) Naccache, R.; Yu, Q.; Capobianco, J. A. *Adv. Opt. Mater.* **2015**, *3* (4), 482.

(16) Ye, X.; Collins, J. E.; Kang, Y.; Chen, J.; Chen, D. T. N.; Yodh, A. G.; Murray, C. B. *Proc. Natl. Acad. Sci. U. S. A.* **2010**, *107* (52), 22430.

(17) Mai, H.-X.; Zhang, Y.-W.; Si, R.; Yan, Z.-G.; Sun, L.; You, L.-P.; Yan, C.-H. *J. Am. Chem. Soc.* **2006**, *128* (19), 6426.

(18) Mai, H.; Zhang, Y.; Sun, L.; Yan, C. *J. Phys. Chem. C* **2007**, *111* (37), 13730.

(19) Li, Z.; Zhang, Y. *Nanotechnology* **2008**, *19* (34), 345606.

(20) Li, C.; Yang, J.; Quan, Z.; Yang, P.; Kong, D.; Lin, J. *Chem. Mater.* **2007**, *19* (20), 4933.

(21) Wang, F.; Wang, J.; Liu, X. *Angew. Chem., Int. Ed.* **2010**, *49* (41), 7456.

(22) Zhao, J.; Lu, Z.; Yin, Y.; McRae, C.; Piper, J. a; Dawes, J. M.; Jin, D.; Goldys, E. M. *Nanoscale* **2013**, *5* (3), 944.

(23) Fischer, S.; Johnson, N. J. J.; Pichaandi, J.; Goldschmidt, J. C.; Van Veggel, F. C. J. M. *J. Appl. Phys.* **2015**, *118* (19), 193105.

(24) Johnson, N. J. J.; van Veggel, F. C. J. M. *Nano Res.* **2013**, *6* (8), 547.

(25) Kömpe, K.; Borchert, H.; Storz, J.; Lobo, A.; Adam, S.; Möller, T.; Haase, M. *Angew. Chem., Int. Ed.* **2003**, *42* (44), 5513.

(26) Zhang, F.; Che, R.; Li, X.; Yao, C.; Yang, J.; Shen, D.; Hu, P.; Li, W.; Zhao, D. *Nano Lett.* **2012**, *12* (6), 2852.

(27) Vetrone, F.; Naccache, R.; Mahalingam, V.; Morgan, C. G.; Capobianco, J. A. *Adv. Funct. Mater.* **2009**, *19* (18), 2924.

(28) Wu, X.; Zhang, Y.; Takle, K.; Bilsel, O.; Li, Z.; Lee, H.; Zhang, Z.; Li, D.; Fan, W.; Duan, C.; Chan, E. M.; Lois, C.; Xiang, Y.; Han, G. *ACS Nano* **2016**, *10* (1), 1060.

(29) Ma, C.; Xu, X.; Wang, F.; Zhou, Z.; Liu, D.; Zhao, J.; Guan, M.; Lang, C. I.; Jin, D. *Nano Lett.* **2017**, *17* (5), 2858.

(30) Xie, X.; Gao, N.; Deng, R.; Sun, Q.; Xu, Q.-H.; Liu, X. *J. Am. Chem. Soc.* **2013**, *135* (34), 12608.

(31) Huang, X.; Han, S.; Huang, W.; Liu, X. *Chem. Soc. Rev.* **2013**, *42* (1), 173.

(32) Chen, X.; Peng, D.; Ju, Q.; Wang, F. *Chem. Soc. Rev.* **2015**, *44* (44), 1318.

(33) Hemmer, E.; Acosta-Mora, P.; Méndez-Ramos, J.; Fischer, S. *J. Mater. Chem. B* **2017**, *5* (23), 4365.

(34) Chen, G.; Ågren, H.; Ohulchanskyy, T. Y.; Prasad, P. N. *Chem. Soc. Rev.* **2015**, *44* (6), 1680.

(35) Rinkel, T.; Raj, A. N.; Dühnen, S.; Haase, M. *Angew. Chem., Int. Ed.* **2016**, *55* (3), 1164.

(36) Mai, H.; Zhang, Y.; Sun, L.; Yan, C. *J. Phys. Chem. C* **2007**, *111* (37), 13721.

DOI: 10.1021/jacs.7b07496
J. Am. Chem. Soc. 2017, 139, 12325−12332

(37) Johnson, N. J. J.; Korinek, A.; Dong, C.; Van Veggel, F. C. J. M. *J. Am. Chem. Soc.* **2012**, *134*, 11068.
(38) Dühnen, S.; Haase, M. *Chem. Mater.* **2015**, *27* (24), 8375.
(39) Yi, G.-S.; Chow, G.-M. *Chem. Mater.* **2007**, *19* (3), 341.
(40) Li, X.; Shen, D.; Yang, J.; Yao, C.; Che, R.; Zhang, F.; Zhao, D. *Chem. Mater.* **2013**, *25*, 106.
(41) Johnson, N. J. J. J.; Van Veggel, F. C. J. M. *ACS Nano* **2014**, *8* (10), 10517.
(42) Levy, E. S.; Tajon, C. A.; Bischof, T. S.; Iafrati, J.; Fernandez-Bravo, A.; Garfield, D. J.; Chamanzar, M.; Maharbiz, M. M.; Sohal, V. S.; Schuck, P. J.; Cohen, B. E.; Chan, E. M. *ACS Nano* **2016**, *10* (9), 8423.
(43) Zhang, C.; Lee, J. Y. *ACS Nano* **2013**, *7* (5), 4393.
(44) Peng, H.-Y.; Ding, B.-B.; Ma, Y.-C.; Sun, S.-Q.; Tao, W.; Guo, Y.-C.; Guo, H.-C.; Yang, X.-Z.; Qian, H.-S. *Appl. Surf. Sci.* **2015**, *357*, 2408.
(45) Liu, D.; Xu, X.; Du, Y.; Qin, X.; Zhang, Y.; Ma, C.; Wen, S.; Ren, W.; Goldys, E. M.; Piper, J. A.; Dou, S.; Liu, X.; Jin, D. *Nat. Commun.* **2016**, *7*, 10254.
(46) Zhang, Y.; Huang, L.; Liu, X. *Angew. Chem., Int. Ed.* **2016**, *55* (19), 5718.

DOI: 10.1021/jacs.7b07496
J. Am. Chem. Soc. 2017, 139, 12325−12332